Energy dependence of the deformed optical potential for neutron scattering from ^{54,56}Fe and ^{58,60}Ni up to 80 MeV

R. S. Pedroni,* C. R. Howell, G. M. Honoré,† H. G. Pfutzner,
R. C. Byrd,‡ and R. L. Walter
Department of Physics, Duke University, Durham, North Carolina 27706
and Triangle Universities Nuclear Laboratory, Durham, North Carolina 27706

J. P. Delaroche
Service de Physique et Techniques Nucléaire, Centre d'Études de Bruyères-le-Châtel, 91680 Bruyères-le-Châtel, France
and Triangle Universities Nuclear Laboratory, Durham, North Carolina 27706
(Received 27 May 1988)

Angular distributions of the analyzing power $A_y(\theta)$ have been measured for neutron elastic scattering and for neutron inelastic scattering to the first 2_1^+ states of ^{54,56}Fe and ^{58,60}Ni at 10 MeV, and for ^{54}Fe and ^{58}Ni at 14 and 17 MeV. The differential cross sections $\sigma(\theta)$ for the same processes were measured at 17 MeV for ^{54}Fe and ^{58}Ni. These measurements have been combined with other measurements of $\sigma(\theta)$ and $A_y(\theta)$ and also with total cross sections to form a sizable data set for incident neutron energies up to 80 MeV. This data set has been described in the context of the coupled channels formalism to determine the energy dependences of the various terms of the deformed optical potential. Some emphasis was placed on investigating the magnitude of the deformation parameter β_{so} of the neutron spin-orbit potential and the possibility that it might be energy dependent.

I. INTRODUCTION

During recent years an intensive effort has been made at the Triangle Universities Nuclear Laboratory (TUNL) to trace the properties of the optical potential for polarized and unpolarized neutrons scattered from spherical and nearly spherical nuclei in the incident energy range from 8 to 14 MeV. For example, it was shown[1] for $n+^{40}$Ca that a precise determination of geometries, energy dependences, and deformation parameters can be achieved, provided that many differential cross section $\sigma(\theta)$, analyzing power $A_y(\theta)$, and total cross section σ_T measurements performed over a broad energy range are combined in a single coupled channel (CC) analysis. A similar broad study of neutron data was made by Finlay *et al.*[2] for $n+^{208}$Pb. In this case the analysis was made in the context of the spherical optical model formalism and concentrated mainly on describing cross section data.

One interesting outcome of such broad analyses is that the interplay between surface absorption and volume absorption can be fairly well mapped. However, characterization of this interplay requires that $\sigma(\theta)$ data be available at incident energies E between 10 and 40 MeV. This necessary condition was fulfilled for ^{40}Ca and ^{208}Pb since complementary $\sigma(\theta)$ measurements covering this energy interval were performed at Ohio University, Michigan State University, and TUNL.

The main purpose of the present CC analysis is to perform a similar, broad investigation of the potential for neutron scattering from ^{45}Fe and ^{58}Ni. This investigation has been made possible in large part by the new $\sigma(\theta)$ and $A_y(\theta)$ measurements for the ground and first 2^+ excited states of ^{54}Fe and ^{58}Ni reported here for 17 MeV. These measurements are among the first to be performed in our laboratory at this relatively high energy. The data base for the CC analysis also include earlier $\sigma(\theta)$ and $A_y(\theta)$ measurements[3–5] performed at TUNL over the energy range from 8 to 14 MeV and $\sigma(\theta)$ measurements from Ohio University.[6,7] The σ_T measurements of Larson *et al.*[8] for Fe and Ni samples of natural abundance are used together with the $\sigma(\theta)$ measurements above 17 MeV to derive an energy-dependent optical potential for the energy range up to 80 MeV. In contrast with the earlier CC analyses[3–5] where the volume absorption W_V was assumed to vary as a linear function of the incident energy, it is assumed here that $W_V(E)$ varies as a Fermi distribution

$$W_V(E)=W_{Vo}\{1+\exp[(E-E_0)/\Delta]\}^{-1}, \quad (1)$$

to ensure that $W_V(E)$ does not take on unreasonable values as E increases up to 100 MeV.

The above measurements performed at 17 MeV have been supplemented with new $A_y(\theta)$ measurements for elastic scattering and inelastic scattering to the first 2^+ excited state (hereafter labeled as 0_1^+ and 2_1^+, respectively) of ^{54}Fe and ^{58}Ni at $E=10$ and 14 MeV. The composite set of ^{54}Fe and ^{58}Ni neutron scattering measurements has been obtained to form a data base for CC calculations which is as complete as possible at the present time. Such a set of $A_y(\theta)$ data was also intended to allow an investigation of the possibility that the deformation parameter β_{so} of the deformed neutron spin-orbit potential[9] is energy dependent. Although a dependence of β_{so} on E is not well understood, a large energy dependence has been suggested[10] in $(\mathbf{p},p')$ scattering from the 2_1^+ level of ^{54}Fe at incident energies between 17 and 25 MeV.

In an additional set of experiments that are also reported here, $A_y(\theta)$ data have been obtained at 10 MeV for the ground state and first 2_1^+ excited state of ^{56}Fe and ^{60}Ni to form a set of $A_y(\theta)$ data at this incident energy for isotopic pairs. No $A_y(\theta)$ measurements at higher incident energies for these two nuclei have been performed because of the prohibitive amount of accelerator time (i.e., about 12 h per datum) presently required to perform such measurements for inelastic scattering with reasonably good statistics. The new $A_y(\theta)$ measurements at 10 and 14 MeV have been performed at angles selected to complement the previous TUNL analyzing power measurements of Refs. 4 and 5. The purpose of these additional measurements for the 2_1^+ state was to permit us to investigate further the dependence of β_{so} on the nuclear structure of these four isotope which lie near the shell closure with N or Z equal to 28.

II. MEASUREMENTS

A. Cross sections

The differential cross-section measurements reported here for 17 MeV are some of the first such data to be obtained at TUNL at this energy. The experimental method represents an extension of the time-of-flight technique described in previous papers.[3,4] Basically, the ion source pulsing system, and detector arrangement are identical to those described in Ref. 3, so only brief comments will be given here. The neutron source reaction is the ^{2}H(d,n)^{3}He and our Monte Carlo simulation, which included the energy loss in the gas cell and the geometry of the scattering arrangement, gave an overall neutron energy spread of 300 keV and a mean energy of 16.93 MeV. The distance from the gas cell to the scatterer was about 10 cm. The four scattering samples used for the work in the present paper ranged in mass from 35 to 50 g and were enriched to better than 98% abundance. Specific details of the scatterers are given in Refs. 3 and 5.

Two detectors are used to measure the scattering yields, one at about 4 m ("right detector") and one at about 6 m ("left detector"). At forward angles the detectors are positioned at equal scattering angles on opposite sides of the beam axis to cancel the angle uncertainty due to a possible misalignment of the deuteron (or resultant neutron) beam axis. Using this method, the average scattering angle is known to within about 0.2°. For other angles, where the angular dependence of $\sigma(\theta)$ is not so severe, the measurements were typically made at alternate angles with each detector, occasionally obtaining an overlap measurement for accuracy and stability tests. Absolute cross-section determination is obtained by normalization to the well-known n-p differential cross section. This is accomplished by making several interspersed measurements of neutron scattering from hydrogen contained in a calibrated polyethylene scatterer. A fixed neutron detector, which monitors the neutron source intensity directly, was used to determine the relative scattering yields at each angle.

A sample time-of-flight spectrum for the 6-m detector is shown in Fig. 1 for ^{58}Ni. The overall time resolution

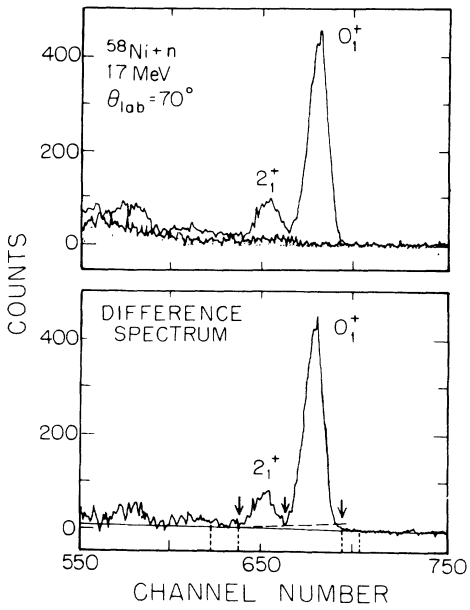

FIG. 1. Time-of-flight spectra for scattering unpolarized 17-MeV neutrons from ^{58}Ni. See text for details.

(full-width at half-maximum) of about 2.2 ns allowed suitable separation of the peaks in both the 6-m and 4-m detectors. Elastic scattering produces the peak labeled 0_1^+ and inelastic scattering to the first excited state at 1.45 MeV produces the 2_1^+ peak. For ^{54}Fe the separation between the peaks for the 0_1^+ state and the 2_1^+ state at 1.41 MeV for ^{54}Fe looked similar, so the spectrum is not included here. The dotted area illustrated in Fig. 1 represents the level of the background measured when the ^{58}Ni target was removed. The lower half of Fig. 1, which shows the yield after subtracting the measured background, indicates that a residual background exists. For separately extracting the yields for elastic and inelastic scattering, a different linear background, intended to represent this residual background, was subtracted from each peak area. These underlying backgrounds are indicated by the solid line at the base of the 0_1^+ peak and the dashed line below the 2_1^+ peak. The arrows indicate the summation limits for extracting the yields.

Multiple-scattering and finite-geometry corrections were applied in the customary TUNL manner. Relative uncertainties on the final $\sigma(\theta)$ data are about 2% to 5% for the elastic scattering cross sections and are typically 10–15% for the 2_1^+ case. The uncertainty on the normalization introduces a scale error of about ±4% for measurements at this energy of 17 MeV. Values of the $\sigma(\theta)$ data have been submitted to the National Nuclear Data Center at Brookhaven National Laboratory.

B. Analyzing powers

Similar methods to those discussed in previous papers[4,5] were employed to measure the $A_y(\theta)$ distributions. Briefly, the ^{2}H(**d**,**n**)^{3}He polarization transfer reaction at 0° served as the source of polarized neutrons. The

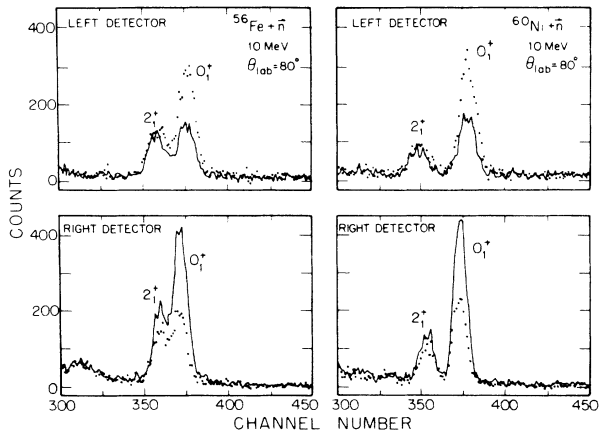

FIG. 2. Time-of-flight spectra for scattering polarized 10-MeV neutrons from ^{56}Fe and ^{60}Ni. The solid line is for neutron beam polarization directed up, dots are for polarization directed down. See text for details.

neutron polarization was typically 0.55. As in the $\sigma(\theta)$ experiments, time-of-flight detection methods were used to resolve the elastic scattering from 2_1^+ scattering. Unlike most of the previous $A_y(\theta)$ measurements at TUNL, the two detectors were positioned at their maximum 4-m and 6-m flight paths for the right and left detectors, respectively, to obtain maximum resolution. However, the corresponding decrease in counting rates meant that high accuracy inelastic scattering data required 12 h at some of the angles. This large amount of accelerator time prohibited us from obtaining greater detail in the structure of the $A_y(\theta)$ distributions for (n,n') at 10 MeV and from obtaining data of the same high accuracy for inelastic scattering in the 14 and 17 MeV experiments with ^{54}Fe and ^{58}Ni.

The data were obtained for all four isotopes at approximately 9.92 MeV and for ^{54}Fe and ^{58}Ni at 13.94 and 16.93 MeV. The corresponding neutron energy spreads were 0.55, 0.39, and 0.30 MeV, respectively. The large energy spread at 10 MeV was employed purposely to obtain useful statistical accuracy for the (n,n') data, while accepting the possible limitations of having poor energy resolution data for the elastic scattering analyses. Time-of-flight spectra at $E=10$ MeV for ^{56}Fe (2_1^+ state at 0.85 MeV) and ^{60}Ni (2_1^+ state at 1.33 MeV) are shown for both detectors in Fig. 2. The solid curves indicate the spectra obtained with the neutron beam polarization oriented in the "up" direction and the dots represent the spectra for the "down" polarization orientation. The large asymmetry for the 0_1^+ yields at this energy and angle are quite evident. The spectra are relatively clean and the resolution is adequate for $A_y(\theta)$ determinations, since in this case only the ratio of yields for the spin-up and spin-down orientations needs to be extracted, and therefore, narrow (identical) windows can be used to find the relative yields. As is conventional at TUNL, in order to avoid some instrumental asymmetries, all $A_y(\theta)$ data were measured with the left and right detectors simultaneously positioned at equal angles on opposite sides of the beam axis. Corrections associated with the finite size of the scatterer were calculated with our Monte Carlo simulation code JANE.

The present $A_y(\theta)$ results at 10 and 14 MeV are compared in Fig. 3 to the earlier Fe data of Floyd *et al.*[4] and in Fig. 4 to the earlier Ni data of Guss *et al.*[5] The solid curves represent fits of the product $\sigma(\theta)\cdot A_y(\theta)$ expressed in a series expansion of associated Legendre polynomials. Not only are the new data consistent with smooth angular dependences, but they are quite compatible with the data from Refs. 4 and 5 previously recorded at TUNL. At 17 MeV no previous data exist for similar comparisons; the data from the present work are shown in Sec. III below. The error bars shown on the $A_y(\theta)$ plots

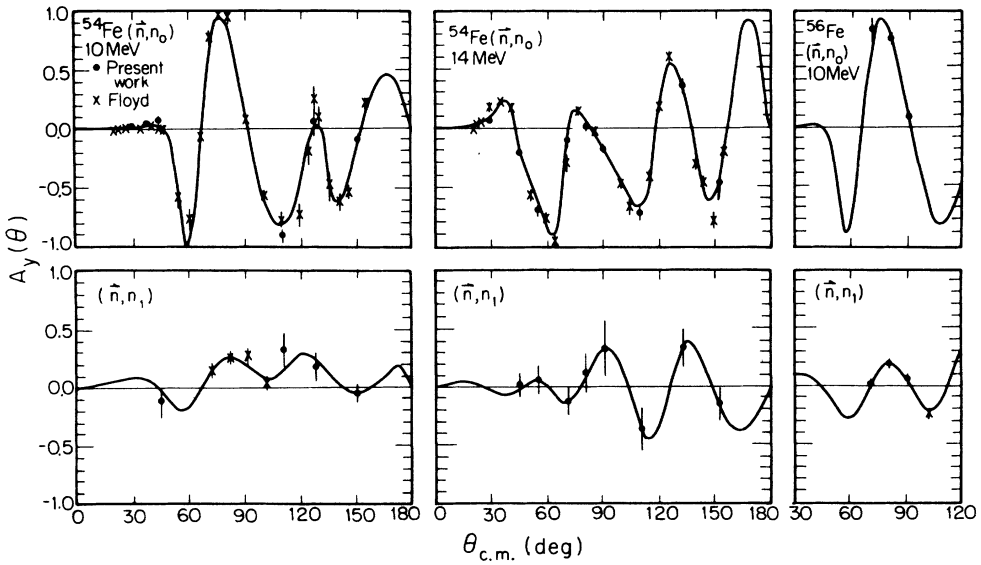

FIG. 3. Present $A_y(\theta)$ data (solid circles) and previous TUNL data (crosses) from Floyd *et al.* (Ref. 4) for 10 and 14 MeV neutron scattering from ^{54,56}Fe.

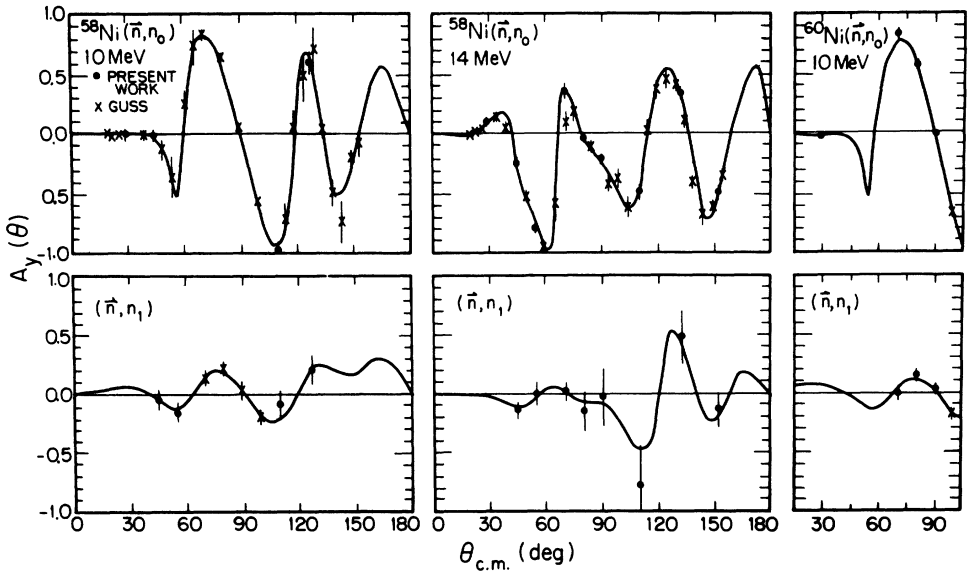

FIG. 4. Present $A_y(\theta)$ data (solid circles) and previous TUNL data (crosses) from Guss *et al.* (Ref. 5) for 10 and 14 MeV neutron scattering from ^{58,60}Ni.

represent all known uncertainties except for a scale uncertainty of about 1.00±0.03 associated with the polarization transfer coefficient for the ^{2}H(**d**,**n**)^{3}He reaction. The $A_y(\theta)$ data have also been transmitted to the National Nuclear Data Center at Brookhaven National Laboratory. Additional details of the $A_y(\theta)$ and $\sigma(\theta)$ experiments, as well as the CC analyses that follow below, are given in the dissertation of Pedroni.[11]

III. COUPLED CHANNELS ANALYSIS

A. Method of analysis

The deformed optical potential for neutron scattering is written as

$$U(\mathbf{r}) = -V_R f(r,a_R,R_R) - iW_V f(r,a_V,R_V) + 4ia_D W_D \frac{d}{dr} f(r,a_D,R_D) - 2i\lambda_\pi^2 [(V_{so}+iW_{so})\nabla f(r,a_{so},R_{so})\times\nabla\cdot\mathbf{s}] , \quad (2)$$

where the strengths of the real potential, the volume and surface absorptions, and the real and imaginary spin-orbit potentials are V_R, W_V, W_D, V_{so}, and W_{so}, respectively. The radial form factors are Woods-Saxon types

$$f(r,a_i,R_i) = \{1+\exp[(r-R_i)/a_i]\}^{-1} ,$$

with

$$R_i = r_i A^{1/3}\left[1+\sum_\mu a^i_{2\mu} Y^2_\mu(\theta,\phi)\right] ,$$

where the angles (θ,ϕ) refer to the center-of-mass system of coordinates. The $a_{2\mu}$ is a quadrupole phonon operator which is related to the vibration amplitude β^i_2 according to a standard definition as given in Ref. 12. The first derivative of $U(\mathbf{r})$ is assumed for the $E2$ transitions between the 0^+_1 and 2^+_1 levels, and for the reorientation $2^+\leftrightarrow 2^+$ terms in the CC calculations performed for ^{58}Ni and ^{56}Fe. The reduced matrix elements used for the reorientation terms were derived[3,5] from the quadrupole moments of the 2^+_1 levels measured in Coulomb excitation measurements.[13-14] In the calculations it is assumed that the deformation lengths $\delta_c = \beta^i_2 r_i A^{1/3}$ are the same for the real and imaginary central potentials. On the other hand, the deformation length δ_{so} for the spin-orbit interaction is allowed to vary with energy and to differ from δ_c.

As stated earlier, because of the wealth of data being described, it was meaningful to introduce a more flexible energy dependence in describing the absorptive potential. The functional form assumed for $W_V(E)$ has been given in Sec. I. For the surface absorption, it was initially assumed that

$$W_D(E) = a(E-\varepsilon_F)^2 \exp\{-[b(E-\varepsilon_F)]\} , \quad (3)$$

where ε_F is the Fermi energy. This $W_D(E)$ behaves as $(E-\varepsilon_F)^2$ near the Fermi energy,[15] and the damping factor $\exp[b(E-\varepsilon_F)]$ ensures that that surface absorption levels off at midenergies and then approaches zero asymptotically. Even though $W_V(E)$ does not have the same functional form as $W_D(E)$, its values near ε_F are chosen to be very small [i.e., $W_V(\varepsilon_F) < 100$ keV)]. For the real central and spin-orbit potentials, the functional forms V_R and $V_{so}(E)$ are those of step 3 in Ref. 5. That is, V_R is linear in E up to 20 MeV and then varies as $\ln E$; $V_{so}(E)$ is linear in E.

The CC calculations were performed using ECIS 79 of Ref. 16. Relativistic kinematics was used for energies above 30 MeV. In the early stage of analysis it was seen that the imaginary spin-orbit potential was of marginal importance, even for describing the $A_y(\theta)$ data. So, in

TABLE I. The optical model parameters obtained in the present analysis of neutron scattering from ^{54}Fe and ^{56}Fe. The units for the potential well strengths are in MeV, and the geometry parameters are expressed in fm. The term ε is equivalent to $(N-Z)/A$. The Fermi energy ε_F is the average Fermi energy for neutrons and has the value of -11.3 MeV for ^{54}Fe and -9.42 for ^{56}Fe.

$V_R=57.89-20.35\varepsilon-0.46E$			$0\le E\le 20$ MeV
$V_R=76.25-20.35\varepsilon-9.2(\ln E)$			$20\le E\le 80$ MeV
$W_V=8.40\{1+\exp[-(E-50.0)/10.0]\}^{-1}$			$0\le E\le 80$ MeV
$W_D(^{54}\text{Fe})=0.0780(E-\varepsilon_F)^2\exp[-0.0750(E-\varepsilon_F)]$			$0\le E\le 12$ MeV
$W_D(^{56}\text{Fe})=0.0677(E-\varepsilon_F)^2\exp[-0.0704(E-\varepsilon_F)]$			$0\le E\le 12$ MeV
$W_D=7.919-14.54\varepsilon-0.082(E-12)$			$12\le E\le 80$ MeV
$V_{so}=6.20-0.015E$			$0\le E\le 80$ MeV
$W_{so}=0.0$			$0\le E\le 80$ MeV
$r_R=1.165$	$r_V=1.165$	$r_D=1.290$	$r_{V_{so}}=1.017$
$a_R=0.656$	$a_V=0.656$	$a_D=0.580$	$a_{V_{so}}=0.600$
$\beta_2(^{54}\text{Fe})=0.20$		$\beta_2(^{56}\text{Fe})=0.24$	

order to reduce the number of parameters involved in Eq. (2), it was decided to set W_{so} equal to zero. The CC analyses have been performed separately for the Ni and Fe isotopes, with an emphasis placed on ^{54}Fe and ^{58}Ni because the TUNL $A_y(\theta)$ experiments concentrated on these two nuclei. Furthermore, the E independent geometries of Ref. 5 and the complex Lane terms given in Refs. 3 and 5 for the Fe and Ni isotopes, respectively, were adopted in the initial step of our CC calculations.

During the early stages of our analysis it was recognized that there is no way to achieve an overall good quality fit to the $\sigma(\theta)$ data across the entire energy range up to 80 MeV by assuming simultaneously the functional forms given in Eq. (1) for $W_V(E)$ and in Eq. (3) for $W_D(E)$. Therefore, it was decided to allow $W_D(E)$ to decrease as a linear function of E beyond some incident energy in the vicinity of 10 MeV.

B. Results

The optimum values found for the deformed and optical potential parameters are shown for Fe in Table I and for Ni in Table II. It can be seen that the potential geometries are the same as in Refs. 3 and 5, except for the absorptive terms. Furthermore, it was possible to hold the deformation parameters at the values obtained in Refs. 3 and 5. The potential depths V_R, $W_V(E)$, and $W_D(E)$ are plotted as a function of the incident energy in Fig. 5 for ^{54}Fe out to an energy of 100 MeV, although the data set only reached to 80 MeV. A slight E dependence was found for V_{so}, but this dependence is much weaker than that reported in Ref. 5 for the Ni isotopes. The sensitivity of the calculations to the deformation length is discussed in Sec. III C. For the calculations described in the present section, $\delta_{so}=\delta_c$ for ^{58}Ni and $2\delta_c$ for ^{54}Fe.

The dependences of the real and imaginary central potentials upon the asymmetry $\varepsilon=(N-Z)/A$ are given in Tables I and II. These dependences cannot be explicitly given for $W_D(E)$ at energies below 12 MeV because the Fermi energy ε_F takes on different values for each nucleus. However, the parametrizations shown for $W_D(E)$ in this energy range have been chosen to closely preserve the dependences on ε found for $E>12$ MeV.

Finally, to a very good approximation the functional

TABLE II. Same as Table I except for neutron scattering from ^{58}Ni and ^{60}Ni. The Fermi energy ε_F has the average value of -10.6 MeV for ^{58}Ni and -9.63 MeV for ^{60}Ni.

$V_R=57.75-21.75\varepsilon-0.46E$			$0\le E\le 20$ MeV
$V_R=76.12-21.75\varepsilon-9.2(\ln E)$			$20\le E\le 80$ MeV
$W_V=8.00\{1+\exp[-(E-50.0)/10.0]\}^{-1}$			$0\le E\le 80$ MeV
$W_D(^{58}\text{Ni})=0.0640(E-\varepsilon_F)^2\exp[-0.0670(E-\varepsilon_F)]$			$0\le E\le 12$ MeV
$W_D(^{60}\text{Ni})=0.0624(E-\varepsilon_F)^2\exp[-0.0681(E-\varepsilon_F)]$			$0\le E\le 12$ MeV
$W_D=7.727-15.54\varepsilon-0.082(E-12)$			$12\le E\le 80$ MeV
$V_{so}=6.20-0.015E$			$0\le E\le 80$ MeV
$W_{so}=0.0$			$0\le E\le 80$ MeV
$r_R=1.165$	$r_V=1.165$	$r_D=1.290$	$r_{V_{so}}=1.017$
$a_R=0.656$	$a_V=0.656$	$a_D=0.580$	$a_{V_{so}}=0.600$
$\beta_2(^{58}\text{Ni})=0.19$		$\beta_2(^{60}\text{Ni})=0.21$	

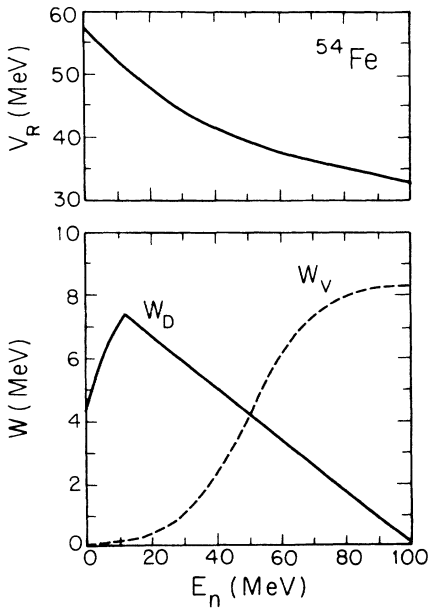

FIG. 5. Plot of V, W_D, and W_V vs incident energy up to 100 MeV for ^{54}Fe.

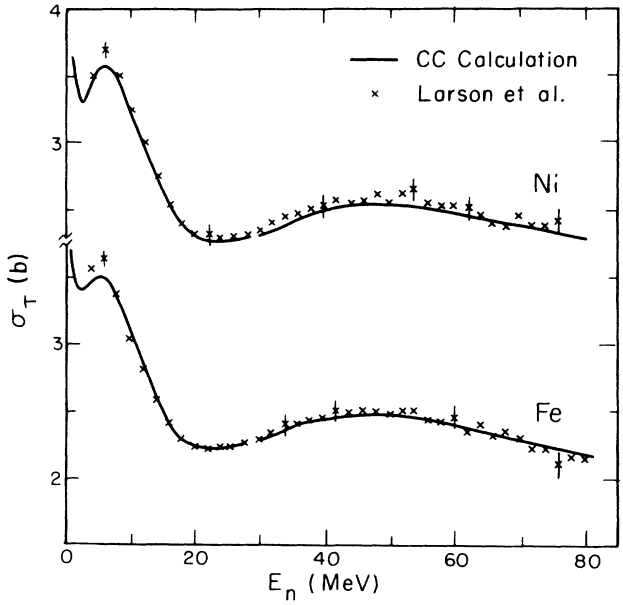

FIG. 6. The total cross section data of Larson *et al.* for samples of Ni and Fe having the natural abundance compared to the CC calculations for ^{58}Ni and ^{54}Fe. The break in the solid line at energies between 30 and 32 MeV is intended to indicate a discontinuity in the calculations when the transition is made to relativistic kinematics at 30 MeV.

form in Eq. (3) that was adopted here for $W_D(E)$ is equivalent to the functional form $W_D(E)=a\sqrt{E}$ that was used, for instance, in Ref. 5 to parametrize the E dependence of the surface absorption below 12 MeV. Taking the average values of the coefficient in the asymmetry terms in Tables I and II for the Fe and Ni isotopes, one can obtain an estimate of these terms that is valid for the Fe-Ni mass region. The values are 21 ± 3 MeV and 15 ± 4 MeV for the real and surface imaginary central potentials, respectively.

The first comparison between experimental results and the CC calculations that we make is for the s- and p-wave strength functions written as S_0 and S_1, respectively, and for the potential scattering radius R'. The new CC results for ^{54}Fe, ^{56}Fe, and ^{58}Ni are only slightly different from those given in Refs. 3 and 5; thus this new analysis does not help to remove the discrepancies observed earlier[3,5] between the measurements of these quantities and the calculations. The same observation can be made for ^{60}Ni: The new R' and S_1 measurements[17] at $E=225$ keV [$R'=5.5\pm0.03$ fm and $S_1=(3.0\pm0.5)\times10^{-5}$] are to be compared with the CC results ($R'=5.56$ fm and $S_1=6.43\times10^{-5}$) calculated for the same incident energy.

Comparisons between the σ_T measurements of Larson *et al.* (Ref. 8), which are averaged over 2 MeV bins, and the present CC calculations are shown in Fig. 6. The uncertainties on these data are about 2% at $E=4$ MeV and increase up to 4% by $E=80$ MeV. Typical error bars are indicated in Fig. 6. Above 8 MeV the agreement between the calculated and measured σ_T is very good. These calculations give better agreement with the data than those which use the deformed optical potential of Ref. 5. In the region between 5 and 8 MeV there is a systematic discrepancy between the data and the curves that has not been explained as yet. For that reason and the problem with S_1 mentioned above, it seems that the optical potential for Fe and Ni presents serious difficulties in the low energy region which deserve further attention. This problem is discussed in Sec. III E.

C. Comparison to $\sigma(\theta)$ data

Comparisons between the calculations and the measurements for ^{58}Ni at 17 MeV for the elastic and inelastic scattering differential cross sections are shown in Fig. 7. Overall, there is quite good agreement between the calculations and the measurements. The CC calculations also compare favorably to the data of Guss *et al.*[5] at 8, 10, 12, and 14 MeV and of Yamanouti *et al.*[6] at 24 MeV. The comparison is not shown here as the CC calculations of the present work and those already shown in Ref. 5 are qualitatively quite similar. One small difference of a systematic nature is that the calculations in Ref. 5 provide better agreement with the elastic scattering data at angles between 30° and 60°, while the present ones are closer to the data between 130° and 160°. Both the present and Ref. 5 calculations for inelastic scattering are also in quite good agreement with the measurements, except in the vicinity of $\theta=120°$ at $E=12$, 14, and 17 MeV, where the calculations overpredict the cross section. We have been unable to eliminate this problem around 120°; neither changing the potential parameters nor adding the coupling to the low-lying 3_1^- state helped. The differences between the CC calculations and the measurements in the vicinity of 120° might be tied with our incomplete treatment of the dynamic properties of these

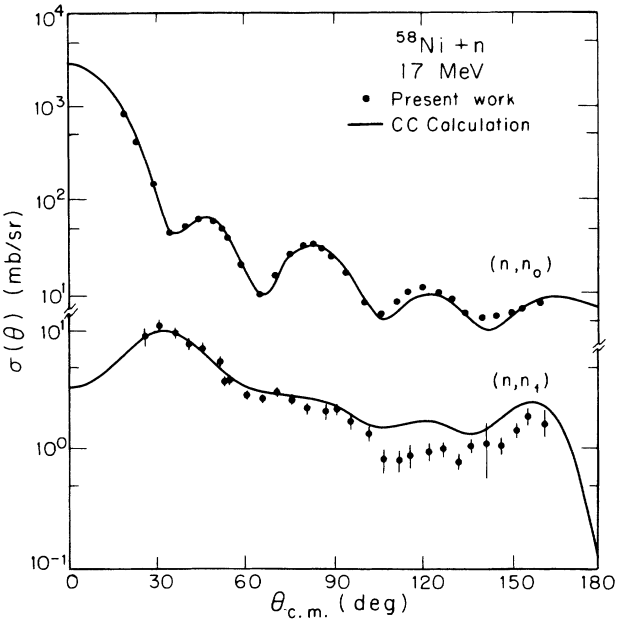

FIG. 7. Comparison of the present measurement at 17 MeV and CC calculations of $\sigma(\theta)$ for scattering to the 0_1^+ and the 2_1^+ states of ^{58}Ni.

nuclei. The possible effects of coupling to $E2$, $T=0$ giant resonances, which are located at an excitation energy between 13 and 17 MeV, might influence the calculations in a way that gives a better description of the data, but this was not investigated in the present analysis.

The data obtained in the present work for ^{54}Fe at 17 MeV are compared to the CC calculations in Figs. 8 and 9, along with comparisons for data obtained previously at other energies. The dotted lines shown at 8 MeV indicate the sum of the CC calculation (direct interaction contribution) and the compound nucleus (CN) contribution calculated[18] using the code CINDY. At the higher energies the CN contribution is negligible. As in the case of ^{58}Ni, the CC calculations agree reasonably well with the ^{54}Fe data, especially considering the wide energy range described by our model. One distinction between the comparison for inelastic scattering is that for ^{54}Fe the data between 10 and 12 MeV lie above the calculation near $\theta=120°$, which is opposite to the discrepancy discussed above for ^{58}Ni. [Although not shown here, the calculated $\sigma(\theta)$ is not very sensitive to the change in δ_{so} from 1.0 to 2.0 δ_c; that is, the difference in the discrepancies near 120° for the two nuclei are not caused by our different choices of δ_{so}.] Inclusion of the CN contribution at 8 MeV causes the calculations for ^{54}Fe (and also ^{54}Ni) to overpredict the measured $\sigma(\theta)$ for elastic scattering (see Fig. 8). On the other hand, the data for inelastic scattering in Fig. 9 favor the magnitude of the calculated CN contribution. We do not believe that errors in the measurements[3] are the cause of this apparent contradiction.

D. Comparison to A_y data

The $A_y(\theta)$ measurements for elastic scattering from ^{54}Fe and ^{58}Ni are shown in Figs. 10 and 11 and for inelas-

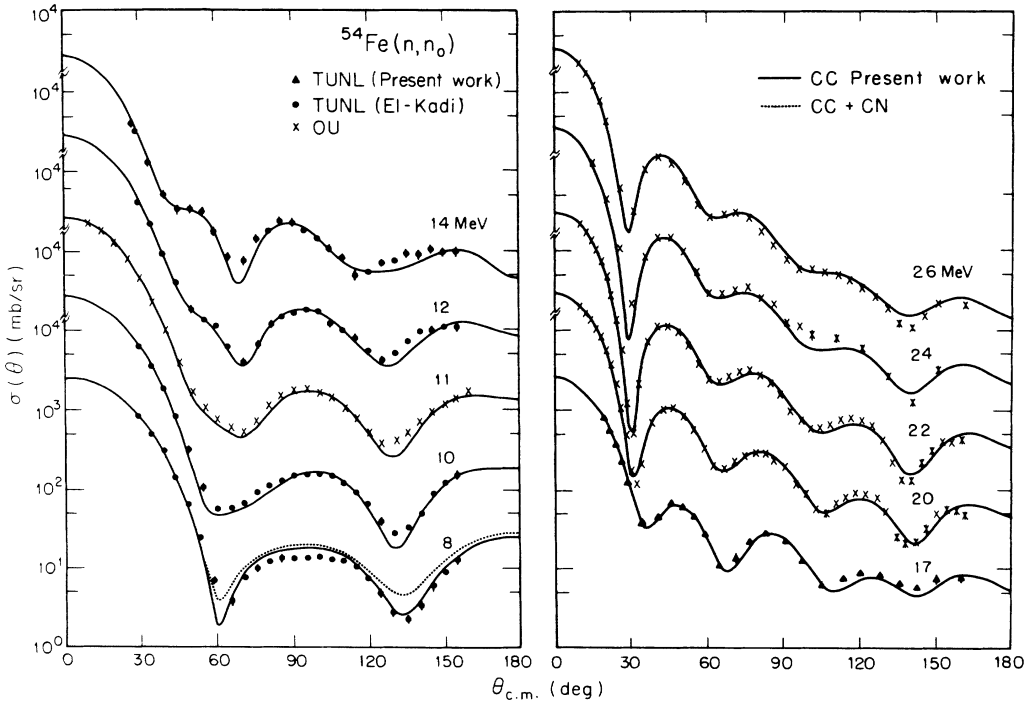

FIG. 8. Comparison of the data and CC calculations for $\sigma(\theta)$ for neutron elastic scattering from ^{54}Fe. The dotted curves at 8 MeV represent the sum of the compound nucleus and the CC contributions. Present measurements are shown by the triangles at 17 MeV. Data from earlier work are also shown: Solid circles are from Ref. 3 and crosses are from Ref. 7.

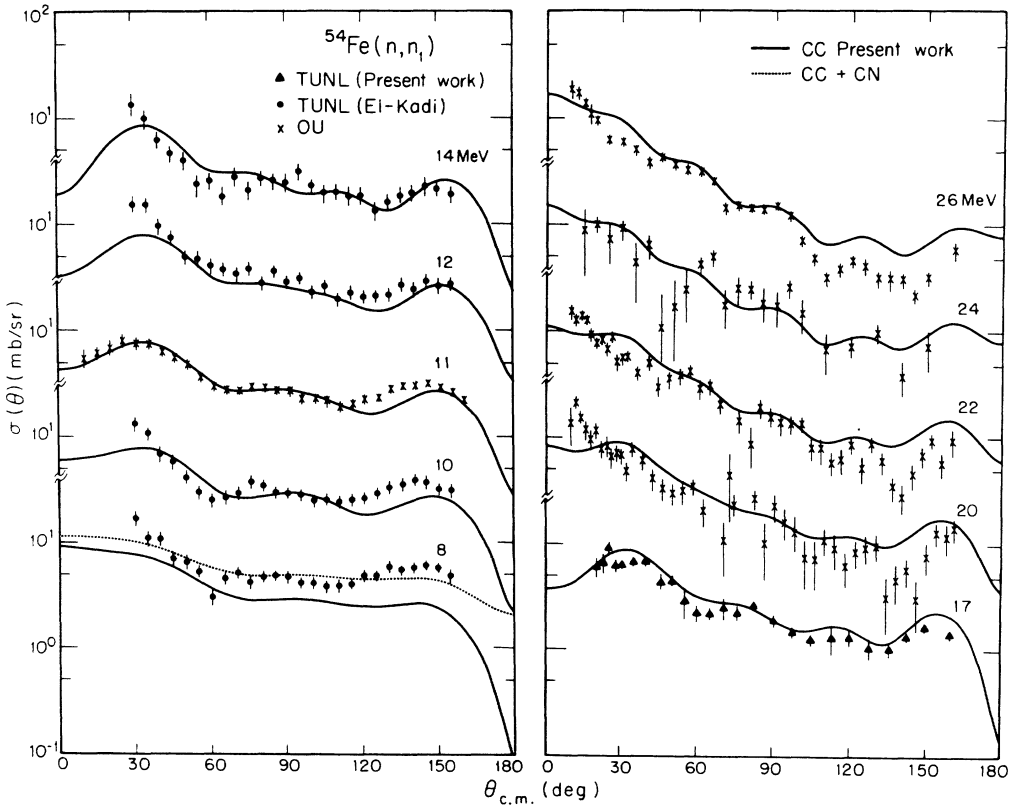

FIG. 9. The data for neutron inelastic scattering to the 2_1^+ state of ^{54}Fe compared to CC calculations. See caption of Fig. 8.

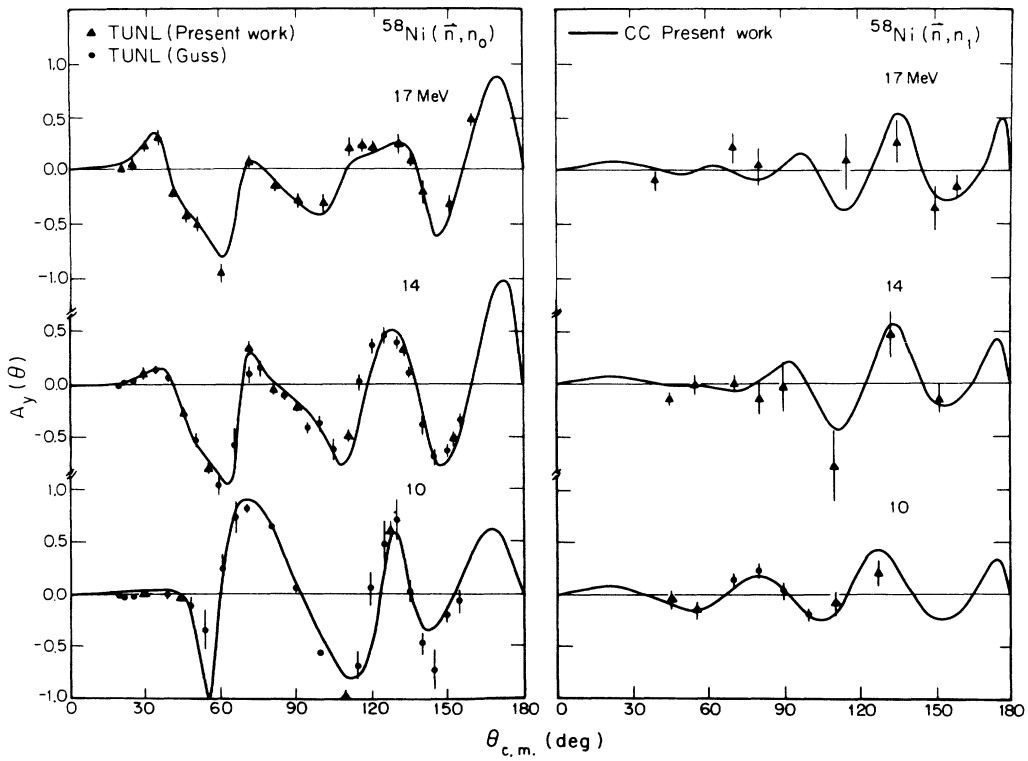

FIG. 10. Comparison of $A_y(\theta)$ data to CC calculations for elastic scattering and inelastic scattering to the 2_1^+ state of ^{58}Ni. Present data are indicated by the triangles.

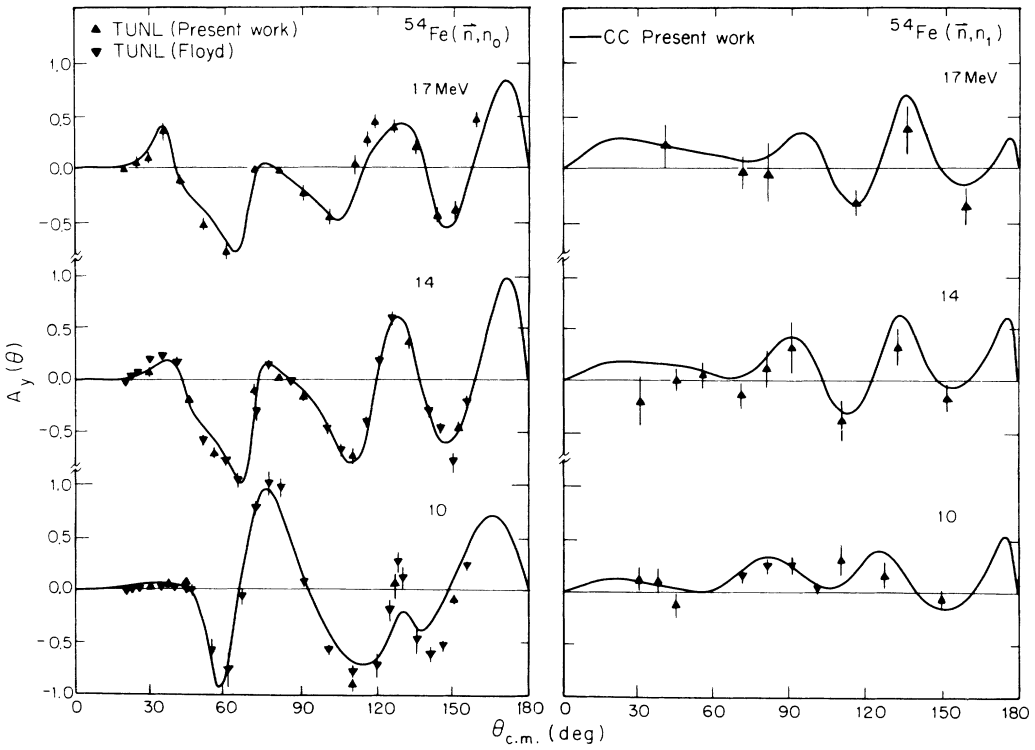

FIG. 11. Comparison of $A_y(\theta)$ data to CC calculations for elastic scattering and inelastic scattering to the 2_1^+ state of ^{54}Fe. Present data are indicated by the upright triangles.

tic scattering to the 2_1^+ levels of ^{54,56}Fe and ^{58,60}Ni in Figs. 10–14. There is quite good overall agreement between the CC calculations and the measurements for elastic scattering. All the calculations for ^{58}Ni shown as solid curves in Figs. 6, 7, and 10 have been performed with the condition that $\delta_{so}=\delta_c$. For ^{54}Fe the calculations in Figs. 8, 9, and 11 were made with the condition that $\delta_{so}=2\ \delta_c$ at all energies; this value is consistent with the earlier finding of Floyd *et al.*[4] and Guss *et al.*[5] Figures 12–14 illustrate the large sensitivity of the CC predictions of $A_y(\theta)$ for the 2_1^+ excited state variations of δ_{so}. As δ_{so} is increased from 0 to 2.0 δ_c, the nature of the sensitivity is unaltered when the incident energy is increased from 10 to 17 MeV. As can be seen from these figures for $A_y(\theta)$, there is good overall agreement between all the inelastic scattering measurements and the CC calculations when $\delta_{so}=\delta_c$, except for ^{54}Fe at 10 MeV, which prefers $\delta_{so}=1.6\delta_c$. However, due to the relatively large uncertainties on the $A_y(\theta)$ measurements for inelastic scattering at the higher energies, it is not possible to claim to have found definite evidence that δ_{so} for ^{54}Fe is energy dependent; a value of $\delta_{so}=1.4\delta_c$ adequately represents all the data. [We note that Van Hall *et al.*[10] found that δ_{so} for ^{54}Fe(p,p') varied between 3.0 and 1.5 times δ_c as the proton energy increased from 17 to 25 MeV.] It should be noted that the few data points for $A_y(\theta)$ reported in our earliest paper[19] on inelastic scattering from ^{54}Fe and ^{58}Ni are included in the plots shown here and still stand as reliable values; however, the present CC calculations are more complete and supersede those in Ref. 19.

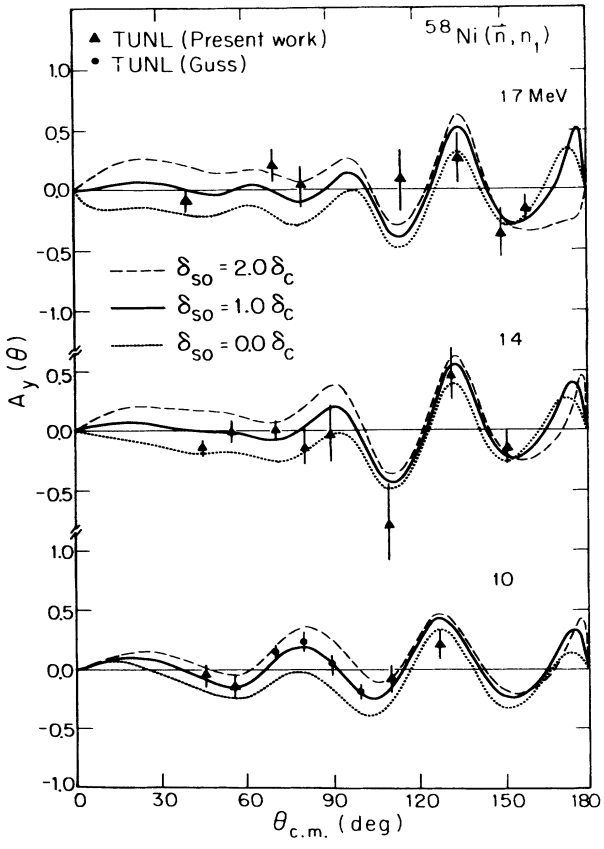

FIG. 12. Sensitivity of the CC calculations for variations in δ_{so} for neutron inelastic scattering to the 2_1^+ state of ^{58}Ni.

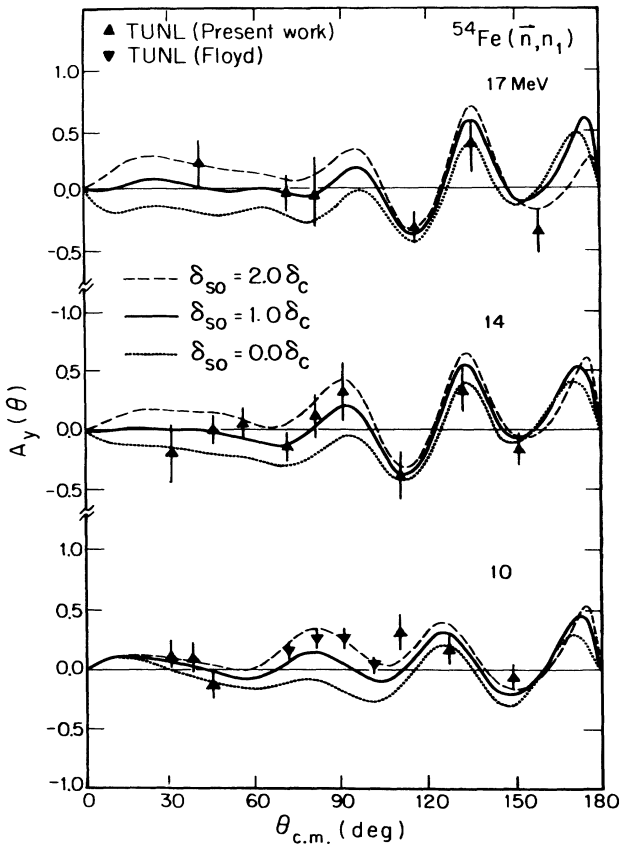

FIG. 13. Sensitivity of the CC calculations to variations in δ_{so} for neutron inelastic scattering to the 2_1^+ state of ^{54}Fe.

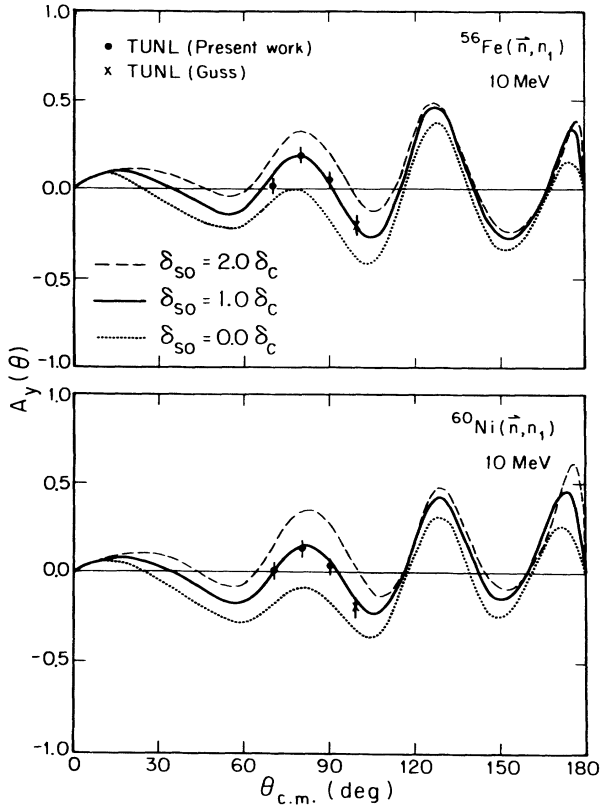

FIG. 14. Sensitivity of the CC calculations to variations in δ_{so} for neutron inelastic scattering to the 2_1^+ state of ^{56}Fe and ^{60}Ni at 10 MeV. Earlier data (crosses) are from Guss *et al.* in Ref. 19 and Fig. 9 of Ref. 5.

E. Discussion

Although our main emphasis was the study of differential cross sections and analyzing powers at $E > 8$ MeV, a look at the lower energy range reveals deficiencies in the optical potential parametrization shown in Tables I and II. This weakness has already been mentioned for σ_T and S_1 in Sec. III B. Another problem is evident at $E = 8$ MeV where the elastic scattering cross sections are overpredicted for ^{54}Fe (see dotted curve in Fig. 8) and for ^{58}Ni.

A preliminary effort has been made to try to track the origin of these deficiencies. For instance, for ^{58}Ni we have made sensitivity calculations for σ_T, in which V_R is allowed to depart at low energies from the linear energy dependence given in Table II. An improved description of σ_T measurements[20] below 6 MeV (see dashed curve in top half of Fig. 15) is achieved by using the representation of V_R shown as a dashed curve in lower half of Fig. 15. We have also tried to improve the description of $\sigma(\theta)$ for elastic scattering at lower half of 8 MeV by changing the geometry of the real potential. Significant improvements (now shown here) are obtained by increasing the real potential radius by 5%. These preliminary results are encouraging, but a thorough series of calculations must be performed to decisively determine if the geometry parameters need to be E dependent and if V_R departs from linearity as E decreases toward very low

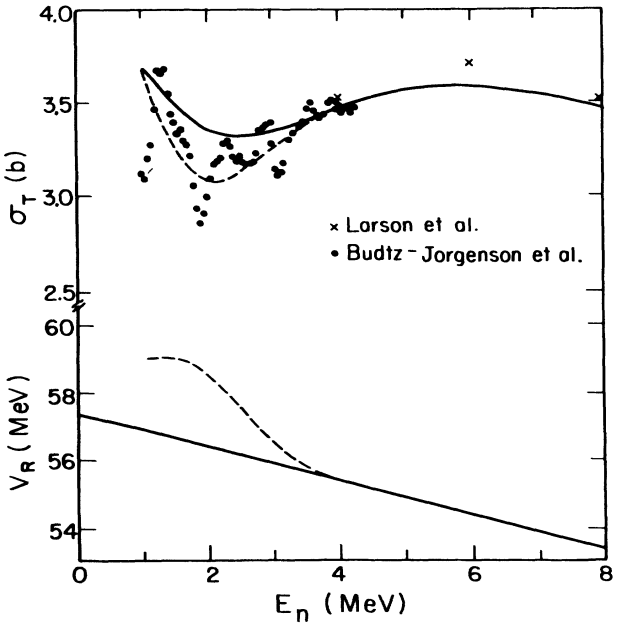

FIG. 15. Top half: Total section for ^{58}Ni calculated using V_R from Table I (solid curve) and using modified V_R (dashed curve). Data are for ^{58}Ni (dots) and naturally abundant Ni (crosses) from Refs. 21 and 8, respectively. Bottom half: Strength of real potential as function of energy according to Table I (solid curve) and to modified form (dashed curve).

values. Such work is underway by two of the present authors (C.R.H. and J.P.D.).

IV. CONCLUSIONS

Neutron scattering data were obtained for ^{54}Fe and ^{58}Ni for $A_y(\theta)$ from 10 to 17 MeV and $\sigma(\theta)$ at 17 MeV. These data were combined with other scattering and reaction data to determine energy-dependent optical potentials for neutron energies up to 80 MeV. A good overall description of the data is achieved. Although the present analysis does not bring any firm evidence of a need for an imaginary spin-orbit potential, the exclusion of this term was not explored exhaustively.

From the $A_y(\theta)$ measurements for inelastic scattering, no evidence exists for an energy-dependent deformation parameter for the spin-orbit term of the $n+^{58}$Ni potential. Furthermore, this spin-orbit deformation length is found to have a magnitude equal to that of the central potential. For ^{54}Fe and data suggest that δ_{so} decreases from about $1.6\delta_c$ to $1.0\delta_c$ as E increases from 10 to 17 MeV, although an energy independent value of $\delta_{so} \simeq 1.4\delta_c$ cannot be excluded. An energy independent value is at variance with (p,p') scattering results, which indicate that δ_{so} drops rapidly from $3.0\delta_c$ to $1.5\delta_c$ as the incident proton energy increases from 17 to 25 MeV. In addition to these $A_y(\theta)$ measurements for inelastic scattering to the 2_1^+ states of ^{54}Fe and ^{58}Ni, complementary data for ^{56}Fe and ^{60}Ni were obtained at 10 MeV. For these nuclei, it was found that $\delta_{so} \simeq \delta_c$, similar to the observation for ^{58}Ni.

Our deformed optical model analyses, based on the assumption that geometries are independent of energy, present deficiencies at incident energies below 10 MeV. The origin of these deficiencies is presently not well understood. Preliminary sensitivity calculations in which the geometry and depth of the real potential are varied from the values shown in Tables I and II lead to improvements. It would be valuable to extend this CC study of the behavior at low energies to examine the connection between the energy dependence of the geometry parameters and the need to modify V_R to include a correction for the dispersion relation associated with $W(E)$.

The data reported here along with the earlier TUNL $A_y(\theta)$ and $\sigma(\theta)$ data for the Fe and Ni isotopes form a unique set of neutron data for this region of the periodic table and therefore provide a special test for microscopic folding models, for instance, of the type discussed by Dietrich and Petrovich.[21] Microscopic analyses of similar sets of TUNL data for other nuclei are underway in collaboration between one of us (R.L.W.) and Dietrich and Hansen of LLNL, and neutron scattering from the present nuclei will be included in the near future.

ACKNOWLEDGMENTS

We are grateful to P. P. Guss for discussions and his assistance in conducting the 10 MeV measurements. We are also grateful to D. C. Larson for releasing the total cross-section measurements prior to publication. This work was supported in part by the U. S. Department of Energy, Office of High Energy and Nuclear Physics, under Contract No. DE-AC05-76ER01067.

*Present address: Department of Physics, Ohio University, Athens, OH 45701.

†Present address: Division of Radiation Physics, Duke University Medical Center, Durham, NC 27706.

‡Present address: Physics Division, Los Alamos National Laboratory, Los Alamos, NM 87545.

[1]G. M. Honoré, W. Tornow, C. R. Howell, R. S. Pedroni, R. C. Byrd, R. L. Walter, and J. P. Delaroche, Phys. Rev. C **33**, 1129 (1986), and references therein.

[2]R. W. Finlay, J. R. M. Annand, T. S. Cheema, J. Rapaport, and F. S. Dietrich, Phys. Rev. C **30**, 796 (1984).

[3]S. M. El-Kadi, C. E. Nelson, F. O. Purser, R. L. Walter, A. Beyerle, C. R. Gould, and L. W. Seagondollar, Nucl. Phys. **A390**, 509 (1982).

[4]C. E. Floyd, P. P. Guss, R. C. Byrd, K. Murphy, R. L. Walter, and J. P. Delaroche, Phys. Rev. C **28**, 1498 (1983).

[5]P. P. Guss, R. C. Byrd, C. E. Floyd, C. R. Howell, K. Murphy, G. Tungate, R. S. Pedroni, R. L. Walter, J. P. Delaroche, and T. B. Clegg, Nucl. Phys. **A438**, 187 (1985).

[6]Y. Yamanouti, J. Rapaport, S. M. Grimes, V. Kulkarni, R. W. Finlay, D. Bainum, P. Grabmayr, and G. Randers-Pehrson, in *Proceedings of International Conference on Nuclear Cross Sections for Technology*, edited by J. L. Fowler, C. H. Johnson, and C. D. Bowman (NBS publication NBS SP **594**, 1980), p. 146.

[7]S. Mellema, R. W. Finlay, F. S. Dietrich, and F. Petrovich, Phys. Rev. C **28**, 2267 (1983); S. Mellema, Ph.D. dissertation, Ohio University (1983).

[8]D. C. Larson, D. M. Hetrick, and J. A. Harvey, Bull. Am. Phys. Soc. **25**, 543 (1980).

[9]H. Sherif and J. S. Blair, Phys. Lett. **26B**, 489 (1968); J. Raynal, *The Structure of Nuclei, Trieste Lectures 1971* (IAEA, Vienna, 1971), p. 75.

[10]J. P. van Hall, J. P. M. G. Melssen, S. D. Wassenaar, O. J. Poppema, S. S. Klein, and G. J. Nijgh, Nucl. Phys. **A291**, 63 (1977).

[11]R. S. Pedroni, Ph.D. dissertation, Duke University (1986), available from University Microfilms, Ann Arbor, MI.

[12]T. Tamura, Rev. Mod. Phys. **37**, 679 (1965).

[13]M. J. Levine, E. K. Warburton, and D. Schwalm, Phys. Rev. C **23**, 244 (1981).

[14]A. Christy and O. Hausser, Nucl. Data Tables **11**, 281 (1972).

[15]C. Mahaux and H. Ngo, Nucl. Phys. **A378**, 205 (1982).

[16]J. Raynal, IAEA Report No. IAEA-SMR-9/8, 1972, p. 75.

[17]R. Winters, C. H. Johnson, and A. D. MacKellar, Phys. Rev. C **31**, 384 (1985).

[18]E. Sheldon (private communication).

[19]P. P. Guss, C. E. Floyd, K. Murphy, C. R. Howell, R. S. Pedroni, G. M. Honore, H. G. Pfutzner, G. Tungate, R. C. Byrd, R. L. Walter, and J. P. Delaroche, Phys. Rev. C **25**, 2854 (1982).

[20]C. Budtz-Jorgensen, P. T. Guenther, A. B. Smith, and J. F. Whalen, Z. Phys. A **306**, 265 (1982).

[21]F. S. Dietrich and F. Petrovich, *Neutron-Nucleus Collisions, A Probe of Nuclear Structure*, edited by J. Rapaport, R. W. Finley, S. M. Grimes, and F. S. Dietrich, AIP Conference Proceeding No. 124 (AIP, New York, 1985), p. 90.